Peer-reviewed version available at *Sensors* **2019**, *19*, 5038; doi:10.3390/s19225038

Article

Compact Inner-Wall Grating Slot Microring Resonator for Label-Free Sensing

Hongjun Gu [1,2], He Gong [1,2], Chunxue Wang [1], Xiaoqiang Sun [1], Xinbin Wang [1], Yunji Yi [1], Changming Chen [1], Fei Wang [1] and Daming Zhang [1,*]

[1] State Key Laboratory of Integrated Optoelectronics, College of Electronic Science and Engineering, Jilin University, 2699 Qianjin Street, Changchun 130012, China; guhj12@mails.jlu.edu.cn; 29878671@qq.com; 531944121@qq.com; sunxq@jlu.edu.cn; xibinwang@jlu.edu.cn; yiyj@jlu.edu.cn; Chencm@jlu.edu.cn; wang_fei@jlu.edu.cn;

[2] College of Information Technology, Jilin Agricultural University, 2888 Xincheng Street, Changchun 130118, China;

* Correspondence: zhangdm@jlu.edu.cn; Tel.: +86-431-8516-8097

Abstract: In this paper, we present and analyze a compact inner-wall grating slot microring resonator (IG-SMRR) with the footprint of less than 13 μm × 13 μm on the SOI platform for label-free sensing, which comprises a slot microring resonator (SMRR) and inner-wall grating (IG). Its detection range is significantly enhanced without the limitation of the free spectral region (FSR) owing to the combination of SMRR and IG. Structural parameters of IG and SMRR are investigated and optimized for favorable transmission properties. The simulation results shows that the IG-SMRR has an ultra-large quasi-FSR of 84.6 nm, and the concentration sensitivities of sodium chloride solutions and D-glucose solutions are up to 960.61 pm/% and 933.06 pm/%, respectively. The investigation on the combination of SMRR and IG is a valuable exploration of label-free sensing application for ultra-large detection range and ultra-high sensitivity in future.

Keywords: microring resonator; inner-wall grating; slot waveguide; label-free; bulk sensing

---

1. Introduction

Label-free optical sensors have been investigated extensively in many applications, such as medical diagnostics, drug detection, food security, pesticide residue detection, environmental monitoring, homeland defense, etc. In the optical sensing applications, two detection strategies, label-based detection and label-free detection are implemented [1]. By comparison, the former suffers from the complex labeling procedures and relatively long assay time, and the latter can be chosen as an alternative for relatively easy and cheap sensing scenarios [2].

In recent decades, a silicon-on-insulator (SOI) platform has been recognized as a favorable candidate due to its compatibility with well-established complementary metal oxide semiconductor (CMOS) manufacturing technology. SOI waveguide can offer high refractive index (RI) contrast that permits strong light mode field confinement and compact bends (down to 1.5 μm bending radius approaching the theory limit) [3]. The optical sensing devices based on the SOI platform have been widely studied, such as Mach-Zehnder interferometer sensors [4], Fabry-Perot resonance sensors [5], surface plasmon sensors [6,7], microring/microdisk resonator sensors [8-11] and grating sensors [12]. The MRR with high qualify factor (Q-factor) enables lights to circle the rings scores of times before being lost, which provides an equivalently long light-matter interaction distance. Therefore, the attractive sensitivity of the optical MRR sensor can be achieved. In addition, the MRR sensor with smaller footprints needs less amount of analyte and is easily integrated in the sensing arrays.

For MRR sensor, two typical interrogation approaches, intensity interrogation and wavelength interrogation [13], have been utilized. The detection range of the former is too small, which is suitable for the relatively lower RI variation of analyte. The latter as the popular detection method can satisfy the actual production demand. The low sensitivity of MRR sensor based on traditional strip waveguide is around 70 nm/RIU [14], and the reason is that the lights trapped in the SOI waveguide cores cannot interact fully with the matter. The SMRR with much light in the slot can enhance the light-analyte interaction. Hence, the SMRR sensor has higher sensitivity. However, the detection range of MRR sensor based on the wavelength shift-dependent is severely constrained by the small FSR. In order to enlarge the detection range, some schemes, such as serially coupled double MRRs [15], the MRR with bent contra-directional couplers [16], Mach-Zehnder interferential couple MRR [17], grating-coupled silicon MRR [18] and angular grating MRR [19] are investigated to expand the FSR. These schemes can enlarge the FSR, but the sensitivities of the above schemes are relativity lower than the sensitivity of SMRR.

In this paper, we present a compact optical label-free sensor based on IG-SMRR to acquire the ultra-large detection range and ensure the high sensitivity. The sensor adopts all-pass filter SMRR, in the inner-wall of which integrated by a grating on an SOI platform. Lumerical MODE Solutions is utilized to simulate the related parameters and sensing performance of the device. The relations between the side mode suppression ratio (SMSR), the extinction ratio (ER), the Q-factor and the structural parameters are investigated. Taking the sodium chloride solutions and D-glucose solution as the top cladding layer, the sensing characteristics of the optical label free sensor are demonstrated.

2. Structure Design and Operation Principle

2.1 Structure design

The 3D schematic of the proposed sensing device is shown Figure 1 (a). The SOI wafer is adopted as the waveguide material with 220 nm Si on a 2 μm SiO_2 substrate. Homogeneous sensing is implemented in this paper, so the sensor device is immersed in aqueous solutions. Naturally, pure water is chosen as the top cladding in the process of determining the geometric parameters of waveguides. This homogeneous sensing case can be easily extended to surface sensing applications by covering thin adsorbed analyte for the top cladding in the calculation. The bent radius (R) of the SMRR is designated as the distance between the center of the rings and the middle of the slot, and set to 5.8 μm. The gap width between the bus and the ring waveguide is denoted as W_{gap}. Other geometric parameters are depicted in Figure (a) and Figure (b). The ring and bus waveguide have the same slot width (W_{slot}). The strip waveguide width W and the slot width W_{slot} are set to 210 nm and 100 nm respectively, which enables an extremely strong restriction of the electric field with the mode confinement factor of over 30% [20]. The etched IG have the azimuthal period (Λ) of about 964 nm, azimuthal width (l_g) and the duty cycle (F) (ratio of silicon block to the period). The structure of the gratings is achieved by etching quasi-rectangular region ($l_g \times H_g$) from the inner-wall of the ring waveguide. Here, H_g is radial height of the etched fragment of the grating.

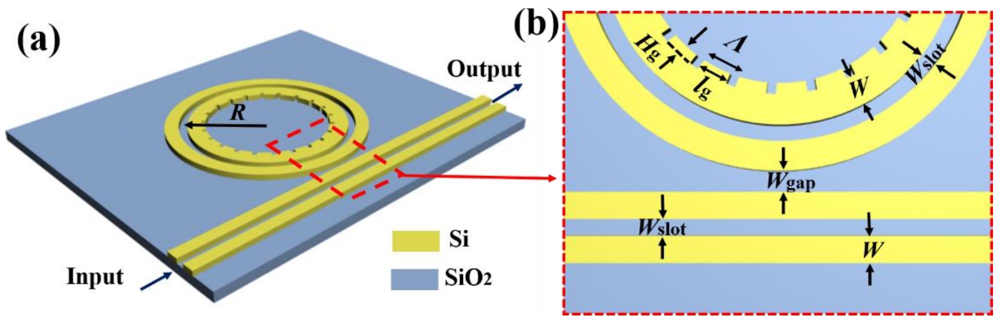

Figure 1. (a) 3D Schematic of the proposed device. **(b)** Top view of the IG-MRR in the coupling region.

2.2 Operation principle

The resonance equation of SMRR can be expressed:

$$2\pi R n_{eff} = m\lambda_{res}, m = 1, 2, 3, ... \quad (1)$$

Preprints (www.preprints.org) | NOT PEER-REVIEWED | Posted: 17 October 2019 doi:10.20944/preprints201910.0199.v1

Peer-reviewed version available at Sensors 2019, 19, 5038; doi:10.3390/s19225038

where, R is the ring radius, n_{eff} is effective RI, m (positive integer) is the azimuthal resonant order, and λ_{res} is the resonant wavelength.

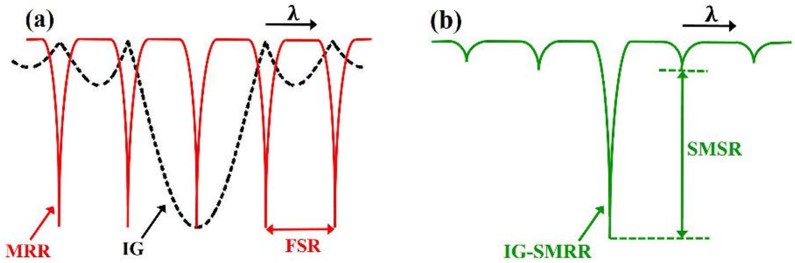

Figure 2 Demonstration of the operating principle. (a) The spectral responses of the SMRR and the IG. (b) The spectral response of the IG-SMRR.

The operating principle of the designed sensor is demonstrated in Figure 2, in which the spectral responses of SMRR, IG and IG-SMRR are described. Obviously, the detection range of sensor is severely restricted by the FSR. The SMRR is filtered by IG with the wavelength-selective characteristic. The detection range of the sensor gets broadened due to the side-mode suppression. The side-mode suppression ratio (SMSR) is optimized by optimizing the etching depth of the IG.

3. Results and Discussion

Mode Solutions software of Lumerical Inc. [21] is utilized to construct the device model and calculate the spectral responses of the sensor. A tunable laser of TE-polarization (the fundamental mode, TE_0) is injected into the bus waveguide. The mode field distribution is calculated by using Finite Difference Eigenmode (FDE) solver as shown in Figure 3. The varFDTD solver collapses a 3D geometry into a 2D set of effective indices that can be solved with 2D FDTD (usually regarded as 2.5D), which ensures the high calculation accuracy and saves much memory and simulation time. The spectral responses of the proposed sensor are carried out by the varFDTD solver. In the process of the following parameter optimization, pure water is acted as the top cladding.

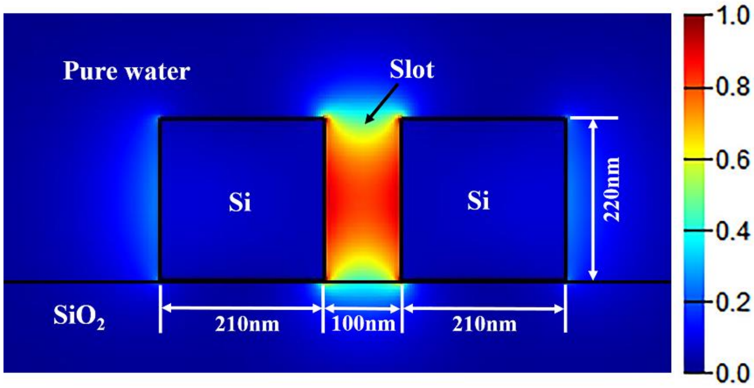

Figure 3 Mode field distribution of the slotted waveguide

The output spectra can be expressed as:

$$T = 10\lg\frac{P_{out}}{P_{in}} \quad (2)$$

where P_{in} and P_{out} are the power flow integrals at the input and output ports, respectively. Q-factor can be calculated from the expression:

$$\text{Q-factor} = \frac{\lambda_{res}}{\text{3dB bandwidth}} \quad (3)$$

where λ_{res} is resonant wavelength of MRR.

3.1 Optimization of Parameters

Preprints (www.preprints.org) | NOT PEER-REVIEWED | Posted: 17 October 2019 doi:10.20944/preprints201910.0199.v1

Peer-reviewed version available at *Sensors* **2019**, *19*, 5038; doi:10.3390/s19225038

High sensitivity of the optical label-free sensor is vital in the practical measuring application. Extinction ration (ER) and Q-factor are two key parameters, which determine the transmission spectrum properties of IG-SMRR, and further influence the sensitivity. Intrinsic propagation loss and coupling loss are main loss resources of the IG-SMRR. SOI waveguide can neglect radiation loss bending loss for R > 3 μm owing to high index contrast [22]. The scattering power loss is mainly caused by IG (less than 13%) [23]. In this case the coupling loss dominates the total loss, and a small W_{gap} (less than 200 nm) can effectively decrease coupling loss [24]. Fig. 4 plots the Q-factor and ER as a function of coupling distance W_{gap} (F=90%, H_g=30 nm). ER increases first, then decreases with the increase of W_{gap}, and reach the peak as W_{gap}=140 nm. Q-factor increases rapidly, then tend to be saturated and fluctuate slightly. In this process, the operating states of MRR transit from over coupling to critical coupling with the increase of ER, and then transit from critical coupling to under coupling with the decrease of ER. W_{gap}=140 nm is favorable to gain the maximum of ER and high Q-factor.

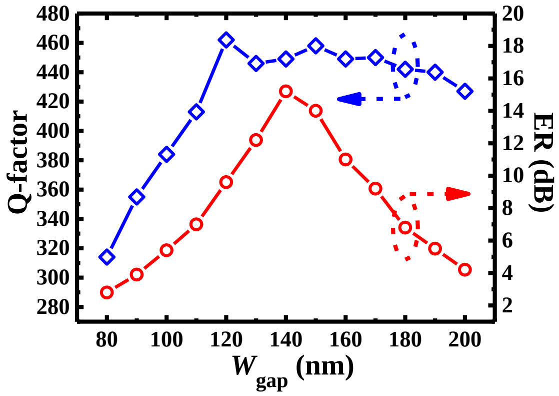

Figure 4 Q-factor and ER as a function of coupling distance *Wgap*

The dependence of Q-factor and ER on the duty cycle F are shown in Figure 5. Variation trend of Q-factor and ER is in the opposite direction. Considering the trade-off between Q-factor and ER, F is set to 95%, and the corresponding Q-factor and ER are 544 and 11dB, respectively.

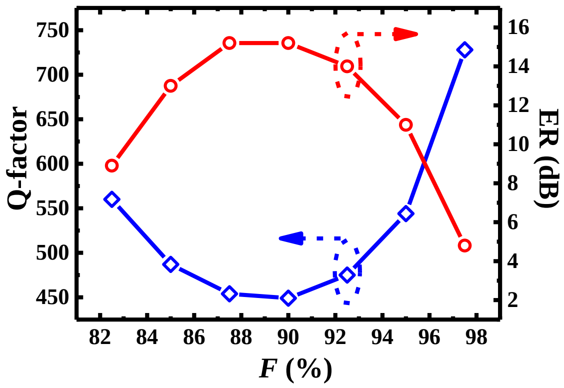

Figure 5 Q-factor and ER as a function of duty cycle F

Q-factor, SMSR and ER as a function of etched depth Hg of the IG are shown in Figure 5 and Figure 6. Here, coupling distance W_{gap} and duty cycle F are fixed at 140 nm and 95%, respectively. Q-factor decreases linearly with the increase of H_g, which is due to the increasing of scattering loss caused by IG. SMSR and ER have similar variation trend. Therefore, considering the trade-off of Q-factor and SMSR, H_g is chosen as 30 nm. The corresponding Q-factor, ER and SMSR are 546, 11 dB and 9.9 dB, respectively. The value of SMSR can fully meet practical needs.

Preprints (www.preprints.org) | NOT PEER-REVIEWED | Posted: 17 October 2019 doi:10.20944/preprints201910.0199.v1

Peer-reviewed version available at *Sensors* **2019**, *19*, 5038; doi:10.3390/s19225038

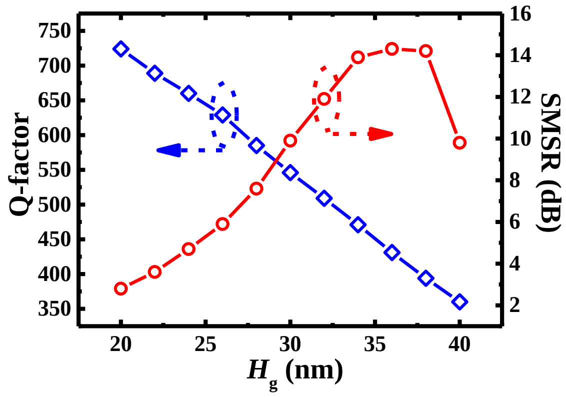

Figure 6 Q-factor and SMSR as a function of etched depth *Hg* of IG

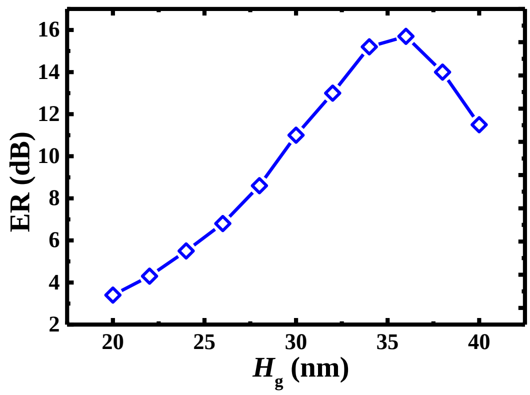

Figure 7 ER as a function of etched depth Hg of IG

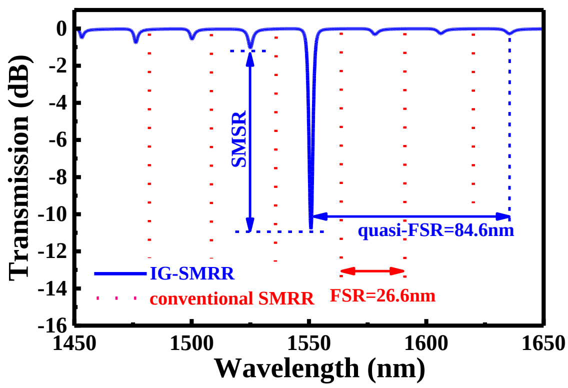

Figure 8 Transmission spectrum of the IG-SMRR (blue solid line) and conventional SMRR (red dashed line)

From the above optimization, several structural parameters of the sensor are determined: coupling distance W_{gap}=140 nm, duty cycle *F*=95% and etched depth H_g=30 nm. And the Q-factor of 546, the ER of 11 dB and the SMSR of 9.9 dB are achieved. As shown in Figure 8, the only one main resonant peak is at 1550.84 nm within the wavelength range from 1450 nm to 1650 nm. The first side mode to the left of main resonant peak has the greatest influence on the spectral characteristic, so it is evaluated by SMSR. The distances between the main resonant peak and its right third suppressed peak is denoted as the quasi-FSR. In the spectrum, the quasi-FSR of the IG-SMRR is 84.6 nm, and the FSR of conventional SMRR is 26.6 nm. Apparently, quasi-FSR is over 3 times of the FSR. Hence, the operating range of the proposed IG-SMRR gets effectively expanded.

3.2 Bulk Sensing Analysis

The sensing principle of IG-SMRR is similar to the optical waveguides. The aqueous solution concentrations as the top cladding are proportional to their RIs. The RI variations of aqueous solution influences the mode optical field interacting the surrounding samples in the slot of the IG-SMRR, which can result in the resonant effective RI variations. Here, the slot plays a crucial role in the sensing process due to the much resonant optical field in it. According to the resonant equation of MRR, the effective RI variations can induce the resonant wavelength shifts. Therefore, the relationship between the solution concentration change and the resonant wavelength shift can be built. The concentration sensitivity [25] of the optical sensor can be defined as:

$$S_C = \Delta\lambda_{res} / \Delta C \tag{4}$$

where ΔC and $\Delta\lambda_{res}$ are the variations of the aqueous solution concentration and resonant wavelength, respectively. This sensitivity means the resonant wavelength shift induced by 1(mass) % concentration.

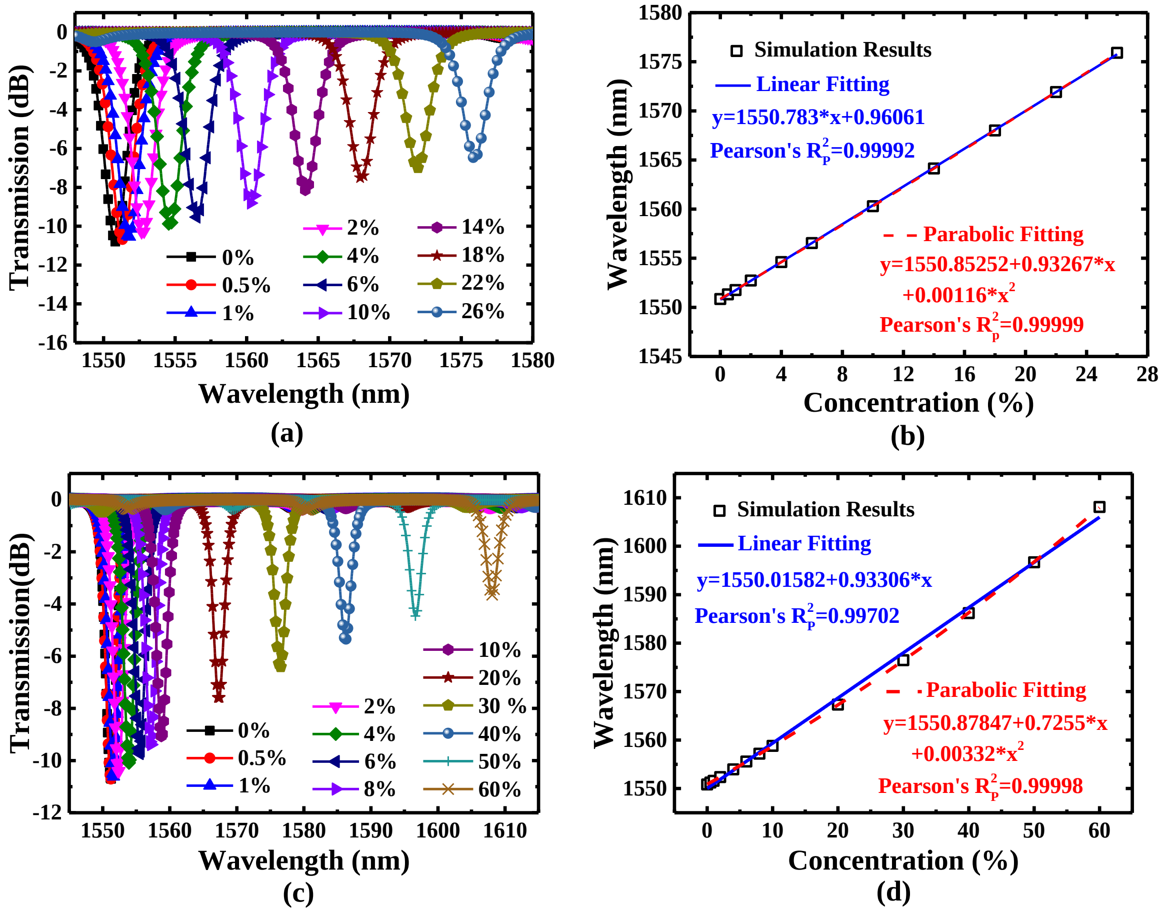

Figure 9 Transmission spectrum of the IG-SMRR for (a) sodium chloride solution, (c) D-glucose solution with different concentrations, and for (b) and (d) corresponding relationships between the resonant wavelength and the solution concentration, respectively.

Table 1. RIs of the Samples (at a temperature of 20℃).

Sample	Concentration (%)	RI
Pure water		1.333
Sodium chloride	0.5-26	1.3339-1.3795
D-glucose	0.5-60	1.3337-1.4394

To demonstrate the bulk sensing characteristic of the IG-SMRR, sodium chloride (NaCl) and D-glucose ($C_6H_{12}O_6$) are designated as samples. Their RIs with different aqueous solution concentrations (mass %) are listed in Table 1 [26].

The conventional MRR can only detect the lower concentration range (<20%) [27] restricted by the small FSR. The IG-SMRR with the wide quasi-FSR can detect the higher concentration (>20%) of the solution due to the large quasi-FSR. The transmission spectra for different concentrations of sodium chloride solutions and D-glucose solutions are shown in Figure 9 (a) and (c), respectively. Figure 9 (b) and (d) illustrates the function relationship between the resonant wavelength and the solution concentration. We utilize the linear and parabolic fittings of the simulation results to discuss the sensing sensitivity and linearity. As shown in Figure 9 (b) and (d), the blue solid and red dashed lines represent the linear and parabolic fittings for the simulation results. A redshift of the resonant wavelength can be observed with the increase of solution concentration. In addition, with the increase of the RIs of samples, the lower index contrast between the solution and the waveguide interfaces results in the smaller intrinsic loss of the waveguide, which induces the decrease of ER [2].

The slope of linear fitting represents the concentration sensitivity of the sensor. The coefficient of determination (R_P^2) is utilized to evaluate the quality of the fitted lines. The sensitivity and R_P^2 are listed in Table 2.

Table 2. Performance of the Sensor with Different Samples for Sensing Application.

Sample	S_c (pm/%)	R_P^2 for Linear Fit	R_P^2 for Parabolic Fit
Sodium Chloride	960.61	0.99992	0.99999
D-glucose	933.06	0.99702	0.99998

As concluded in Table 2, the concentration sensitivities of the sensor for sodium chloride solutions and D-glucose solutions are 960.61 pm/% and 933.06 pm/%, respectively. Compared with [19], both solution concentrations are about 10 times than that of 95.27 pm/% and 95.33 pm/%, respectively. The R_P^2 for linear fit is less than the R_P^2 for parabolic fit, which illustrates that the 2 order parabolic fitting can depict the function relationship between the resonance wavelength and solution concentration more precisely than linear fitting [19,27,28-30]. For the low concentration variations of sodium chloride solutions, R_P^2 for linear fit is 0.99992, which shows the relationship between the resonance wavelength and solution concentration is nearly linear. However, for high concentration range of D-glucose solution, parabolic fitting can be considered. Therefore, a conclusion can be drawn that the linear fitting and parabolic fitting are suitable for the smaller range and larger range concentration detections, respectively.

4. Conclusions

In this work, the SOI IG-SMRR with an ultra-large detection range and a high sensitivity is proposed for label-free sensing. It combines SMRR with IG to enlarge the operating range due to good suppression of side modes. The related parameters are simulated and optimized to get the favorable transmission spectrum. The sensing device based on IG-SMRR has an ultra-large detection range. The concentration sensitivities of sodium chloride solutions and D-glucose solutions are up to 960.61 pm/% and 933.06 pm/%. The numerical analysis shows the linear and parabolic fitting are suitable for low concentration and high concentration detections, respectively. The proposed sensing device with a compact footprint of less than 13 μm × 13 μm is easily integrated with other SOI devices and enables integrated sensor arrays. Therefore, the SOI IG-SMRR combining the benefits of both SMRR and IG is a valuable exploration for micro/nano optical sensing applications in future.

Author Contributions: H.G. (first author) and H.G. (second author) simulated the device and wrote the original draft. C.W. and X.S. conceived the main idea and collected the related literatures. X.W. and Y.Y. analyze the simulation results and directed the simulation work. C.C. and F.W revised the paper. D.M. proofread and submitted the paper.

Funding: This research was funded by the National Natural Science Foundation of China (61575076, 61875069, 61605057 and 61675087), the Science and Technology Development Plan of Jilin Provincial (20190302010GX) and the Fundamental Research Funds for the Central Universities (2019jcxk-59).

Acknowledgments: We thank the Lumerical Inc. for their software support. And we are grateful to the anonymous reviewers contributed to this paper.

Peer-reviewed version available at *Sensors* **2019**, *19*, 5038; doi:10.3390/s19225038

Conflicts of Interest: The authors declare no conflict of interest.

References

1. Fan, X. D.; White, I. M.; Shopova, S. I.; Zhu, H. Y.; Suter, J. D. and Sun, Y. Z. Sensitive optical biosensors for unlabeled targets: A review. *Analytica Chimica Acta* **2008,** 620, 8-26.
2. Sun, L.; Yuan, J. H.; Ma, T.; Sang, X. Z.; Yan, B. B.; Wang, K. R. and Yu, C. X. Design and optimization of silicon concentric dual-microring resonators for refractive index sensing. *Opt Commun* **2017,** 395, 212-216.
3. Xu, Q. F.; Fattal, D. and Beausoleil, R. G. Silicon microring resonators with 1.5-mu m radius. *Opt Express* **2008,** 16, 4309-4315.
4. Dai, D. X. and He, S. L. Highly sensitive sensor based on an ultra-high-Q Mach-Zehnder interferometer-coup led microring. *J Opt Soc Am B* **2009,** 26, 511-516.
5. Yuan, G.; Gao, L.; Chen, Y.; Wang, J.; Ren, P. and Wang, Z. Efficient optical biochemical sensor with slotted Bragg-grating-based Fabry–Perot resonator structure in silicon-on-insulator platform. *Optical and Quantum Electronics* **2014,** 47, 247-255.
6. Nemova, G. and Kashyap, R. Theoretical model of a planar integrated refractive index sensor based on surface plasmon-polariton excitation with a long period grating. *J Opt Soc Am B* **2007,** 24, 2696-2701.
7. Chang, Y. and Jiang, Y. Y. Highly Sensitive Plasmonic Sensor Based on Fano Resonance from Silver Nanoparticle Heterodimer Array on a Thin Silver Film. *Plasmonics* **2014,** 9, 499-505.
8. Zamora V.; Lützow P.; Weiland M. and Pergande D. A Highly Sensitive Refractometric Sensor Based on Cascaded SiN Microring Resonators. *Sensors* **2013,** *13*, 14601-14610.
9. Wei, H. and Krishnaswamy, S. Polymer micro-ring resonator integrated with a fiber ring laser for ultrasound detection. *Opt Lett* **2017,** 42, 2655.
10. Grist, S. M.; Schmidt, S. A.; Flueckiger, J.; Donzella, V.; Shi, W.; Fard, S. T.; Kirk, J. T.; Ratner, D. M.; Cheung, K. C. and Chrostowski, L. Silicon photonic micro-disk resonators for label-free biosensing. *Opt Express* **2013,** 21, 7994-8006.
11. Amiri, I. S.; Ariannejad M. M.; Daud S. and Yupapin, P. High sensitivity temperature sensor silicon-based microring resonator using the broadband input spectrum. *Results Phys* **2018**, *9*, 1578-1584.
12. Ruan, Z.; Shen, L.; Zheng, S. and Wang, J. Subwavelength grating slot (SWGS) waveguide on silicon platform. *Opt Express* **2017,** 25, 18250.
13. Chao, C. Y. and Guo, L. J. Design and optimization of microring resonators in biochemical sensing applications. *J Lightwave Technol* **2006,** 24, 1395-1402.
14. De Vos, K.; Bartolozzi, I.; Schacht, E.; Bienstman, P. and Baets, R. Silicon-on-Insulator microring resonator for sensitive and label-free biosensing. *Opt Express* **2007,** 15, 7610-7615.
15. Kolli, V. R.; Srinivasulu, T.; Hegde, G.; Badrinarayana, T. and Talabattula, S. Design and analysis of serially coupled double microring resonator based force sensor for 1 mu N range measurement. *Optik* **2017,** 131, 1063-1070.
16. Eid, N.; Boeck, R.; Jayatilleka, H.; Chrostowski, L.; Shi, W. and Jaeger, N. A. F. FSR-free silicon-on-insulator microring resonator based filter with bent contra-directional couplers. *Opt Express* **2016,** 24, 29010-29022.
17. Xiong, Y. L. and Ye, W. N. N. Silicon Mach-Zehnder interferometer racetrack microring for sensing. *Proc Spie* **2014,** 8990.
18. Shi, W.; Wang, X.; Zhang, W.; Yun, H.; Lin, C.; Chrostowski, L. and Jaeger, N. A. F. Grating-coupled silicon microring resonators. *Appl Phys Lett* **2012,** 100.
19. Ma, T.; Sun, L.; Yuan, J. H.; Sang, X. Z.; Yan, B. B.; Wang, K. R. and Yu, C. X. Integrated label-free optical biochemical sensor with a large measurement range based on an angular grating-microring resonator. *Appl Optics* **2016,** 55, 4784-4790.
20. Yuan, G. H.; Gao, L.; Chen, Y. R.; Liu, X. L.; Wang, J. and Wang, Z. R. Improvement of optical sensing performances of a double-slot-waveguide-based ring resonator sensor on silicon-on-insulator platform. *Optik* **2014,** 125, 850-854.
21. http://www.lumerical.com.
22. Bogaerts, W.; De Heyn, P.; Van Vaerenbergh, T.; De Vos, K.; Selvaraja, S. K.; Claes, T.; Dumon, P.; Bienstman, P.; Van Thourhout, D. and Baets, R. Silicon microring resonators. *Laser Photonics Rev* **2012,** 6, 47-73.
23. Cai, X. L.; Wang, J. W.; Strain, M. J.; Johnson-Morris, B.; Zhu, J. B.; Sorel, M.; O'Brien, J. L.; Thompson, M. G. and Yu, S. T. Integrated Compact Optical Vortex Beam Emitters. *Science* **2012,** 338, 363-366.

24. Tseng, C. W.; Tsai, C. W.; Lin, K. C.; Lee, M. C. and Chen, Y. J. Study of coupling loss on strongly-coupled, ultra compact microring resonators. *Opt Express* **2013,** 21, 7250-7257.
25. Sang, X.; Yu, C.; Mayteevarunyoo, T.; Wang, K.; Zhang, Q. and Chu, P. L. Temperature-insensitive chemical sensor based on a fiber Bragg grating. *Sensor Actuat B-Chem* **2007,** 120, 754-757.
26. Lide, D. R. Thermochemistry, Electrochemistry, and Solution Chemistry. In *Handbook of chemistry and physics*, 95th ed.; Haynes, W. M. and Bruno, T J.; CRC: California, USA, 2015; pp 130, 142.
27. Girault, P.; Lorrain, N.; Poffo, L.; Guendouz, M. Lemaitre, J. and Lemaitre, J. Integrated polymer micro-ring resonators for optical sensing applications. *J Appl Phys* **2015**, 117, 104504.
28. Liu, Z. B.; Tan, Z. W.; Yin, B.; Bai, Y. L.; Jian, S. S., Refractive index sensing characterization of a singlemode-claddingless-singlemode fiber structure based fiber ring cavity laser. *Opt Express* **2014,** 22, 5037-5042.
29. Xue, L. L.; Yang, L., Sensitivity Enhancement of RI Sensor Based on SMS Fiber Structure with High Refractive Index Overlay. *J Lightwave Technol* **2012,** 30, 1463-1469.
30. Wu, Q.; Semenova, Y.; Wang, P. F.; Farrell, G., High sensitivity SMS fiber structure based refractometer - analysis and experiment. *Opt Express* **2011,** 19, 7937-7944.